Magnetic properties of the low-dimensional spin-$\frac{1}{2}$ magnet α-Cu$_2$As$_2$O$_7$

Y. C. Arango,[1] E. Vavilova,[1,2] M. Abdel-Hafiez,[1] O. Janson,[3] A. A. Tsirlin,[3] H. Rosner,[3] S.-L. Drechsler,[1] M. Weil,[4]
G. Nénert,[5] R. Klingeler,[6] O. Volkova,[7] A. Vasiliev,[7] V. Kataev,[1] and B. Büchner[1]

[1]*Leibniz Institute for Solid State and Materials Research IFW Dresden, D-01171 Dresden, PO BOX 270116, Germany*
[2]*Zavoisky Physical Technical Institute of the Russian Academy of Sciences, 420029, Kazan, Russia*
[3]*Max Planck Institute for Chemical Physics of Solids, D-01187 Dresden, Germany*
[4]*Institute for Chemical Technologies and Analytics, Vienna University of Technology, A-1060 Vienna, Austria*
[5]*Institut Laue-Langevin, Boîte Postale 156, 38042 Grenoble Cedex 9, France*
[6]*Kirchhoff Institute for Physics, University of Heidelberg, D-69120 Heidelberg, Germany*
[7]*Low Temperature Physics Department, Moscow State University, Moscow 119991, Russia*
(Received 21 June 2011; published 20 October 2011)

In this work, we study the interplay between the crystal structure and magnetism of the pyroarsenate α-Cu$_2$As$_2$O$_7$ by means of magnetization, heat capacity, electron spin resonance, and nuclear magnetic resonance measurements as well as density functional theory (DFT) calculations and quantum Monte Carlo (QMC) simulations. The data reveal that the magnetic Cu-O chains in the crystal structure represent a realization of a quasi-one-dimensional (1D) coupled alternating spin-1/2 Heisenberg chain model with relevant pathways through nonmagnetic AsO$_4$ tetrahedra. Owing to residual 3D interactions, antiferromagnetic long range ordering at $T_N \simeq 10$ K takes place. Application of the external magnetic field B along the magnetically easy axis induces the transition to a spin-flop phase at $B_{SF} \sim 1.7$ T (2 K). The experimental data suggest that substantial quantum spin fluctuations take place at low magnetic fields in the ordered state. DFT calculations confirm the quasi-one-dimensional nature of the spin lattice, with the leading coupling J_1 within the structural dimers. QMC fits to the magnetic susceptibility evaluate $J_1 = 164$ K, the weaker intrachain coupling $J_1'/J_1 = 0.55$, and the effective interchain coupling $J_{ic1}/J_1 = 0.20$.

I. INTRODUCTION

Crystals of composition $X_2Y_2O_7$ tend to adopt different structures in which the Y atom may be octahedrally or tetrahedrally coordinated.[1] These systems have been found to exhibit interesting magnetic properties ranging from a geometry induced spin frustration phenomena when X and Y are magnetic metal ions (see, e.g., Ref. 2), to a peculiar interplay between structure and magnetism in those compounds where Y is not magnetic (see, e.g., Refs. 3 and 4). Co, Ni, and Cu diphosphates and divanadates are interesting examples of those latter compounds. In their crystal structure, two YO_4 tetrahedra sharing an oxygen atom usually undergo a transition from a staggered (180°) to a bent Y-O-Y configuration (from thortveitite to dichromate type structure) with the decrease of temperature. A recent comparative band-structure study of copper (II) based pyrocompounds Cu$_2Y_2$O$_7$ (Y = P, As, V)[5] shows that despite having the same basic structural motif, these materials represent completely different magnetic models. Here the change of the nonmagnetic central atom Y in the tetrahedral anion groups YO_4, e.g., from Y = P to V, turns out to be crucial in determining the effective interchain exchange pathways depending on the electronic state (p or d type) of the central Y cation. Moreover, significant variations in the intrachain exchange coupling evidence the subtle effect of the Cu-O-Cu bond angle albeit the basic structural dimerization of Cu$_2$O$_6$ plaquettes is present in all these isostructural compounds. Thus, according to theoretical predictions and experimental data available so far, one can expect that further change of the Y cation might yield a completely new magnetic behavior in this series of materials. The validation of this conjecture would be of specific importance for the development and verification of new magnetic models of low-dimensional Heisenberg quantum magnets which for decades have stood in the focus of intense experimental and theoretical research in condensed matter physics.[6]

Unlike pyrovanadates and even pyrophosphates, the experimental magnetic study of transition metal pyroarsenates, X_2As$_2$O$_7$ (X = Cu, Ni, Co, Mn) is scarce. Only for X_2As$_2$O$_7$ with X = Ni, Co, Mn, early bulk magnetic susceptibility measurements and low-temperature neutron powder diffraction were reported by Buckley *et al.*,[7] whereas there seem to be no experimental results on the copper (II)-based Cu$_2$As$_2$O$_7$ pyroarsenate. Therefore, in view of the expected sensitivity of the magnetic behavior to the type of Y cation, we have carried out a detailed study of magnetic properties of single crystals of α-Cu$_2$As$_2$O$_7$ with different experimental techniques such as magnetization, heat capacity, electron spin resonance (ESR), and nuclear magnetic resonance (NMR) measurements, combined with density functional theory (DFT) calculations and quantum Monte Carlo (QMC) simulations. Indeed, we find that in contrast to other related isostructural compounds, α-Cu$_2$As$_2$O$_7$ represents an experimental realization of coupled spin-1/2 alternating antiferromagentic (AFM) Heisenberg chains where the AsO$_4$ anion groups play an important role for the interchain magnetic exchange. The quasi-one-dimensional magnetic behavior with short-range AFM correlations is dominating over a wide temperature range. At low temperatures, however, secondary magnetic exchange interactions become relevant too, and three-dimensional long-range magnetic order evolves below $T_N \simeq 10$ K. In the magnetically ordered state, the application of moderate magnetic fields $B \simeq 1.7$ T parallel to the crystallographic b axis yields a field induced
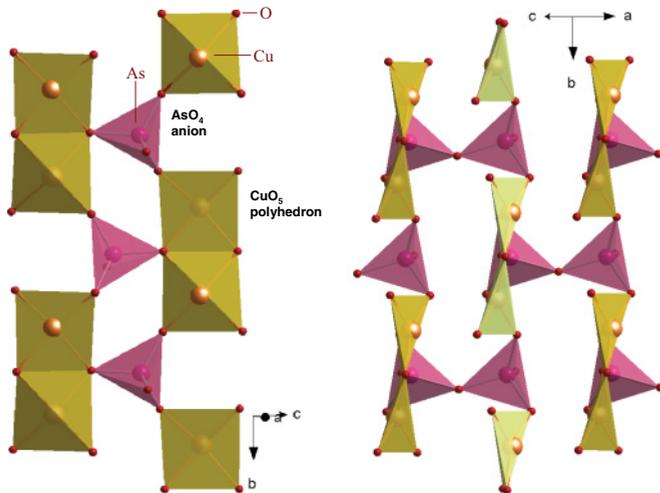
FIG. 1. (Color online) The crystal structure of α-Cu$_2$As$_2$O$_7$. (a) Edge-sharing Cu$_2$O$_6$ plaquettes form structural dimer units along the b axis. The dimers are linked by AsO$_4$ anion groups forming a plane of coupled dimer chains; (b) Side view of the chain planes linked with interjacent As$_2$O$_7$ anions.

reorientation of the spin lattice. Further increase of the magnetic field progressively suppresses spin fluctuations which are evident in the thermodynamic and magnetic resonance response at small fields.

II. CRYSTAL STRUCTURE

Synthesis and characterization of α-Cu$_2$As$_2$O$_7$ single crystals have been reported in Ref. 8. The α-Cu$_2$As$_2$O$_7$ modification crystallizes isotypically with α-Cu$_2$P$_2$O$_7$ and β-Cu$_2$V$_2$O$_7$ structures, belonging to the monoclinic space group $C2/c$ with $a = 7.237(3)$, $b = 8.2557(17)$, $c = 9.780(3)$ Å, $\beta = 111.03(2)^\circ$. The major structural feature of α-Cu$_2$As$_2$O$_7$ is the occurrence of nonplanar Cu$_2$O$_6$ plaquettes (Cu-O-Cu bond of 101.68(8)$^\circ$ and Cu-O bond lengths of 1.92–2.00 Å) forming structural dimers along the crystallographic b direction[8] [Fig. 1(a)]. The AsO$_4$ tetrahedra link these Cu-O-Cu dimers in a chain along the b axis and also interconnect the neighboring chains in the chain plane [Fig. 1(a)]. The chain planes are linked by interjacent pyroarsenate anions As$_2$O$_7$ in a bent As-O-As configuration of 145.9(2)$^\circ$. The fourfold oxygen in-plane coordination of Cu is completed by the fifth oxygen atom from the neighboring plane with a much larger bond length of 2.27 Å, which therefore should only weakly contribute to magnetism.

III. RESULTS AND DISCUSSION

A. Magnetization

Magnetization measurements on a single crystal of α-Cu$_2$As$_2$O$_7$ were carried out in a VSM SQUID magnetometer (Quantum Design) applying the magnetic fields parallel ($B\|b$ axis) and perpendicular ($B\|c$ axis) to the propagation direction of the Cu$_2$O$_6$ plaquettes, respectively. Figure 2 shows the static magnetic susceptibility $\chi = M/B$ in the temperature range 2–350 K at $B = 1$ T. For both field directions, the susceptibility data exhibit a characteristic broad maximum
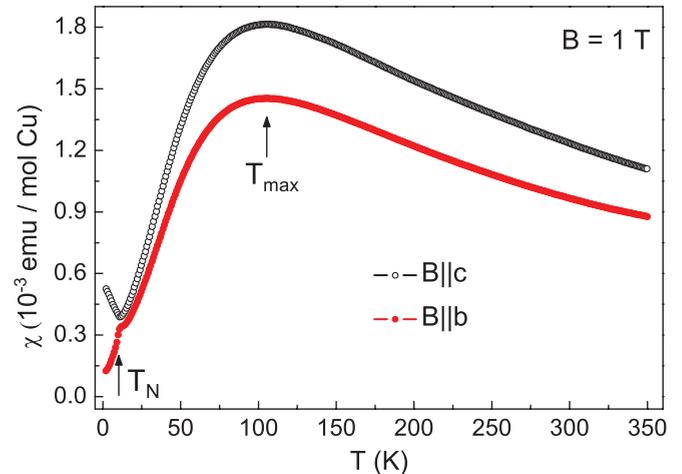
FIG. 2. (Color online) Magnetic susceptibility $\chi = M/B$ of a α-Cu$_2$As$_2$O$_7$ single crystal measured at $B = 1$ T applied along the crystallographic b- and c-axis, respectively.

at about $T \sim 105$ K, which is typically associated with 1D short-range magnetic correlations due to predominant intra-chain magnetic interactions. This value suggests thus a rough estimate of the expected energy scale of the leading exchange constants. At a much smaller temperature $T_N \simeq 10$ K, there is an upturn in $\chi(T)\|c$ and a concomitant kink in $\chi(T)\|b$ evidencing the onset of long-range AFM spin order (see also Figs. 5 and 10). Such a feature and the rapid decrease of $\chi(T)\|b$ down to $T = 2$ K imply the crystallographic b axis being the magnetically *easy* axis.

Further $\chi(T)\|b$ data at various constant applied magnetic fields are shown in Fig. 3. At low field $B < 2$ T, the magnetic specific heat which is proportional to $\partial(\chi T)/\partial T$ exhibits a pronounced λ-like anomaly (Fisher's heat capacity)[9,10] corroborating the scenario of long-range magnetic ordering at $T_N = 10$ K (Fig. 3, inset). Interestingly, the kink in $\chi(T)$ at T_N significantly changes its shape upon application of magnetic field $B > 2$ T. The decrease of $\chi(T)$ below T_N
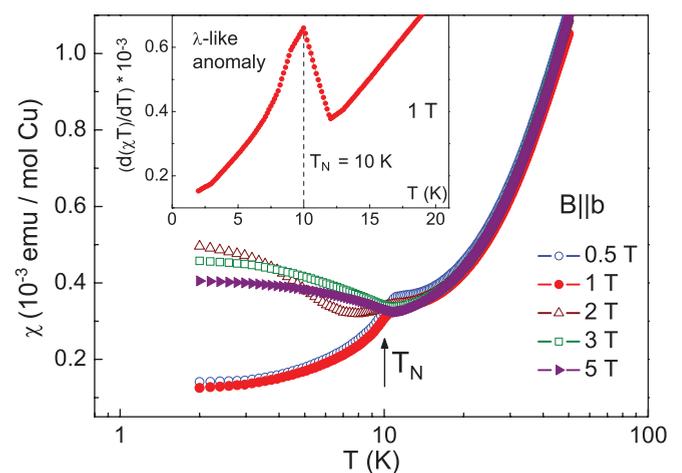
FIG. 3. (Color online) Temperature dependence of the magnetic susceptibility $\chi(T)$. Inset: The pronounced anomaly in the Fisher's heat capacity $\partial(\chi T)/\partial T$ at $B = 1$ T along the b-axis implies long-range magnetic order below $T_N \simeq 10$ K.
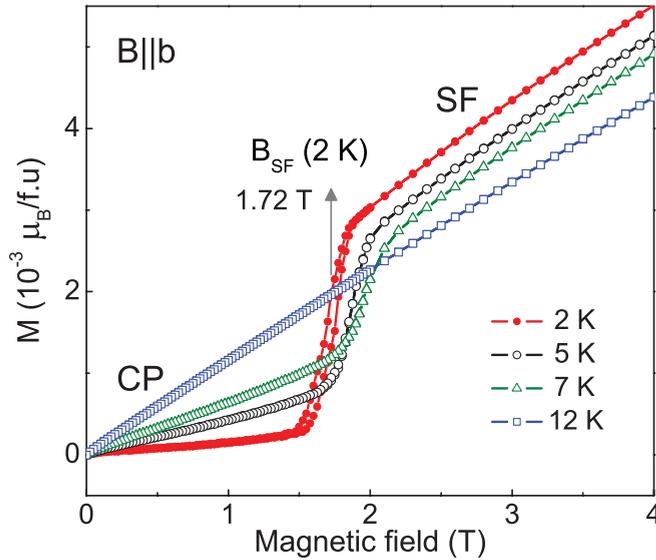
FIG. 4. (Color online) Magnetic field B dependence of the magnetization M for $B \parallel b$ axis at different temperatures slightly above and below T_N. CP and SF denote the presumably collinear phase in the low-field regime and the spin-flop phase at high magnetic fields. The spin-flop transition at $B_{SF} \simeq 1.7\,T$ $(T = 2\,K)$ is associated with the magnetic anisotropy in the system.

turns into a steep upturn at higher fields (Fig. 3). This transformation should be indicative of an additional magnetic phase transition at a critical field in between these values and the development of a field-induced magnetic phase. Such a behavior is indeed clearly visible in the magnetic field dependence of the magnetization M versus $B \parallel b$ (Fig. 4).

Field dependent measurements of magnetization for the $B \parallel b$ axis in Fig. 4 give evidence of a first-order spin-flop transition (SF) below T_N at $B_{SF} \simeq 1.7\,T$ (2 K), in agreement with the $\chi(T)$ data. The spin-flop arises due to the gain in magnetic anisotropy energy of the system above B_{SF} by considering the AF collinear arrangement of Cu^{2+} spins parallel to the b axis at lower fields. The magnetization $M(B)$ data for $B \parallel c$ axis in the field range up to 7 T (not shown) are consistent with a magnetically *hard c* axis, where no anomaly is observed below 12 K.

B. Heat capacity

Figure 5 shows the molar specific heat at $B = 0$ and in different external magnetic fields applied parallel to the b axis. At $B = 0$, the as-measured data do not exhibit a pronounced anomaly at T_N, despite the marked peak in the $\partial(\chi T)/\partial T$ (Fig. 3) clearly indicating anomalous magnetic entropy changes associated with the onset of long-range AFM order. We conclude that, in zero magnetic field, the magnetic entropy changes at T_N are small compared to the phononic ones. In order to highlight this, we have subtracted an arbitrary polynomial background function $f(T) = aT + bT^3$ from the experimental data (cf., e.g., Ref. 11). The resulting data Δc_p are shown in the bottom panel of Fig. 5. At a temperature very close to T_N derived from the susceptibility measurements, the data indicate a kink in Δc_p, at $B = 0$, which is associated with a specific heat anomaly $\Delta c_p < 20\,$mJ$\,$mol$^{-1}\,$K^{-1}. This kink
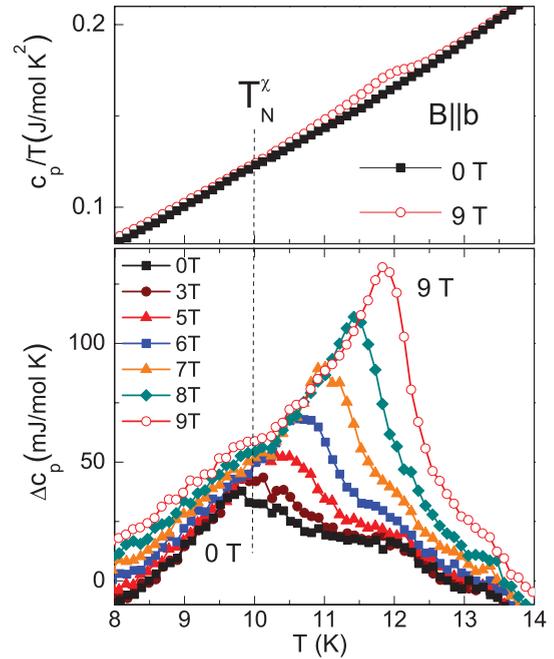
FIG. 5. (Color online) Upper panel: Temperature dependence of the specific heat capacity c_p at $B = 0$ and 9 T; lower panel: Experimental data in different magnetic fields $B \parallel b$-axis after subtraction of an arbitrary polynomial background function $f(T) = aT + bT^3$. T_N^χ indicates the temperature of the anomaly in $\partial(\chi T)/\partial T$ at small fields (cf. Fig. 3).

is hardly affected by small magnetic fields. To be specific, at $B = 5\,$T the kink is found at $T_{max}^c(5\,T) = 10.2\,$K. However, at magnetic fields $B \gtrsim 5\,$T the peak increases in amplitude and shifts to higher temperatures. The growth of the peak suggests the increase of entropy changes associated with the phase transition, i.e., the evolution of a jump-like or a λ-like specific heat anomaly. At $B = 9\,$T, the peak height of the specific heat anomaly amounts to $\simeq 115\,$mJ mol$^{-1}\,$K^{-1}, and the peak maximum occurs at $T_N(9\,T) = 11.9\,$K. The experimental data hence prove a field induced increase of the magnetic entropy changes associated with the onset of long-range magnetic order. The vanishing size of the specific heat anomaly in small magnetic fields, i.e., the absence of significant entropy changes associated with the onset of AFM order, either implies only weak spin order below T_N or the presence of strong spin correlations well above the long-range ordering temperature. The fact that application of moderate external magnetic fields instead of suppression of AFM order yields larger entropy changes associated with the phase transition corroborates the latter scenario. Hence, the specific heat data suggest strong AFM spin fluctuations at low fields. We note that from the present data it is difficult to conclude if additional small shoulder-like features of the $\Delta c_p(T, B = 9\,T)$ curve at $\sim 10\,$K and $\sim 13.3\,$K are of intrinsic nature or arise due to the imperfect subtraction of the nonmagnetic contributions from the total specific heat.

A tentative phase diagram which has been constructed from the magnetization and specific heat data is presented in Fig. 6. In particular, it shows that the spin-flop field which signals the transition from the AFM collinear phase
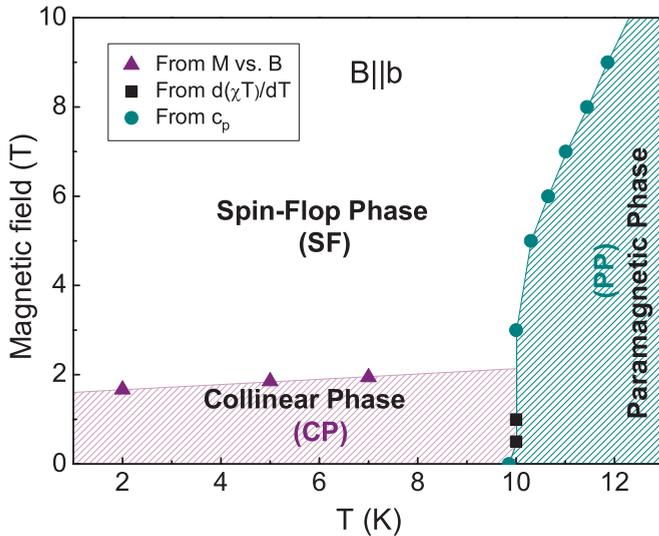
FIG. 6. (Color online) Magnetic phase diagram for α-Cu$_2$As$_2$O$_7$ single crystals according to magnetization and specific heat measurements when applying field along the magnetically *easy b*-axis.

FIG. 7. (Color online) Temperature dependence of the ESR parameters with $B\|b$ at 340 GHz. Main panel: effective g-factor and linewidth, upper and lower curve respectively. Inset: The shift of the ESR resonance line at low temperature reflects the increasing internal magnetic field in the vicinity of the ordered state.

(CP) to the spin-flop phase (SP) is nearly independent of temperature. For a discontinuous phase transition, the slope of the phase boundary is associated with the ratio of the magnetization changes ΔM and the entropy changes ΔS at the phase transition according to $dT/dB = -\Delta M/\Delta S$ (Clausius-Clapeyron relation).[12] Hence, while $\Delta M > 0$, our observation of $dB/dT \simeq 0$ implies the absence of significant entropy changes at the spin-flop transition, as expected for a spin-reorientation in the AFM ordered phase. Quantitatively, at $T = 1.7$ K, we extract $dT/dB \approx 16.2$ K/T and $\Delta M = 2.4 \cdot 10^{-3}$ μ_B/f.u. which yields $\Delta S_{SF} = 0.83$ mJ/(mol K). Consquently, the degree of spin order at high fields/low temperature in the spin-flop phase is very similar to that at zero field/low temperature. Applying the above relation at $T = 5$ K and $T = 7$ K yields decreasing entropy changes at the spin flop transition $\Delta S_{SF}(5\ \text{K}) = 0.64$ mJ/(mol K) and $\Delta S_{SF}(7\text{K}) = 0.45$ mJ/(mol K) as already qualitatively visible from the rather constant slope of the phase boundary while ΔM decreases with temperature.

In contrast, the phase boundary between the paramagnetic and the AFM CP/SF phases implies $dT/dB \approx 0$ for $B \lesssim 5$ T and $dT/dB > 0$ for higher fields. Our data do not allow to judge the exact nature of the specific heat anomaly and to quantitatively estimate the entropy changes or the specific heat jump associated with the phase transition. Firstly, $dT/dB \approx 0$ thermodynamically corresponds to only tiny entropy changes at $T_N(B \lesssim 5$ T) if the Ehrenfest equation[12] (related to a continuous phase transition) and the moderate kink in $\partial M/\partial T$ at the transition are considered. This indeed agrees with our specific data. However, the pronounced *positive* slope at the PP-SF transition appears in qualitative contrast to what is expected for an ordinary AFM phase transition.

C. Electron spin resonance (ESR)

ESR at a frequency of $\nu \sim 10$ GHz has been measured with a commercial X-band spectrometer (Bruker EMX). High-field high-frequency ESR (HF-ESR) measurements have
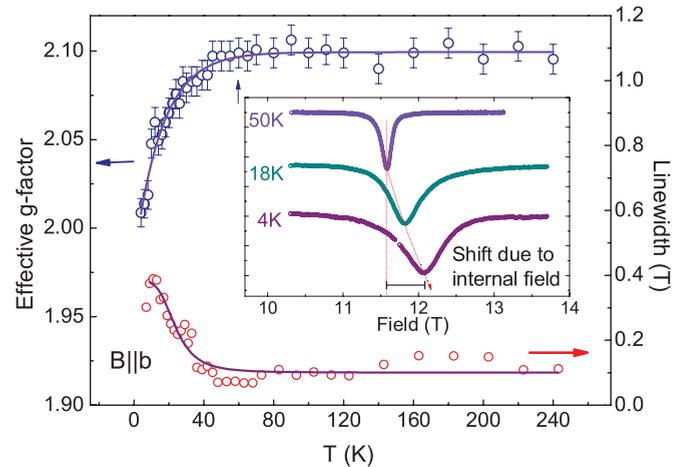
been carried out with the home-made spectrometer on the basis of the Millimeterwave Network Analyzer from AB Millimetré and a 15 T superconducting magnet from Oxford Instruments.[13] A well defined ESR signal of a Lorentzian shape associated with the resonance of Cu^{2+} ($3d^9, S = 1/2$) ions was observed in a broad range of excitation frequencies and temperatures.

The dependence of the position of the ESR line B_{res} on the direction of magnetic field within the crystallographic bc plane has been studied at $\sim$10 GHz at room temperature (not shown). The g factor calculated from this dependence as $g = h\nu/\mu_B B_{res}$ reveals an anisotropy typical for Cu^{2+} ions in a square planar coordination:[14,15] $g_\| \simeq 2.07$ ($B\|b$ along the chains) and $g_\perp \simeq 2.18$ ($B\|c$). Here h is the Planck constant and μ_B is the Bohr magneton.

Temperature dependent HF-ESR measurements were carried out at $\nu = 340$ GHz. For magnetic fields applied along the magnetic *easy* axis ($B\|b$), the g factor is almost temperature independent above $\sim$60 K (Fig. 7) close to a value of $g_\| \simeq 2.09$ which corresponds to $B_{res} \simeq 11.6$ T. A slight discrepancy in the 10 GHz data ($g_\| \simeq 2.07$) is likely due to a slight misorientation of the sample in the HF-ESR probe head. At lower temperature, the g factor drops with decreasing temperature indicating the onset of short-range magnetic ordering when approaching T_N. The shift of the resonance field in this region concomitant with the broadening of the line is apparently due to the growth of local quasistatic internal fields and the increase of the spin correlation length as precursors of the long range magnetic order.

Frequency dependent measurements at $T = 20$ K $> T_N$ show a linear scaling between ν and B (Fig. 8), yielding a g factor $g \simeq 2.07$ from the slope $\partial\nu/\partial B$. Extrapolation of the data to zero field reveals no energy gap for the resonant excitation as expected for an $S = 1/2$ system in the paramagnetic state. An opening of a gap at $B = 0$ is however expected in the magnetically ordered state due to the magnetic anisotropy. For a simple two-sublattice collinear antiferromagnet, the anisotropy gap $\Delta(B = 0)$ is related to the
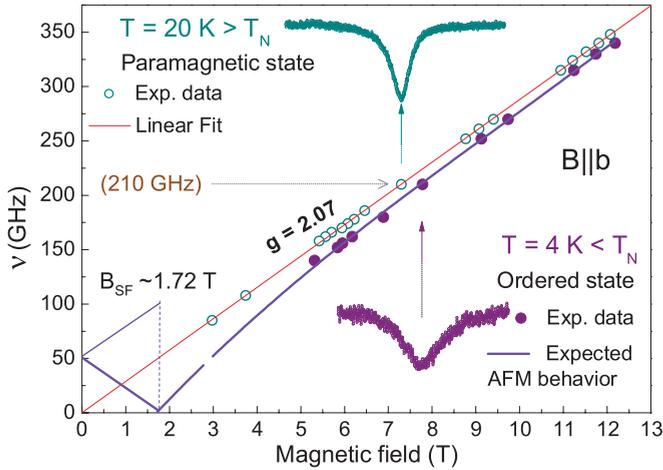
FIG. 8. (Color online) Frequency versus resonance field diagram of the ESR signal in the ordered and paramagnetic states for $B \parallel b$. At 4 K a single resonance mode is observed above ~5 T (solid circles). Solid thin line corresponds to the paramagnetic resonance branch $\nu = g\mu_B B_{res}/h$. Solid thick lines show the expected AFM resonance branches for uniaxial anisotropy with $B \parallel$ *easy b*-axis.[16]

spin-flop field B_{SF} as $\Delta = B_{SF} g\mu_B/h$.[16] With $B_{SF} \simeq 1.7$ T, one obtains $\Delta = 50$ GHz. By applying the field along the *easy b* axis, two resonance modes should develop as sketched in Fig. 8, which collapse at B_{SF}.[16] At $B > B_{SF}$, one resonance branch is expected which approaches the paramagnetic $\nu(B)$ line in strong fields, as shown in Fig. 8. Indeed at high fields a well defined resonance mode has been detected at $T = 4$ K $< T_N$, which follows closely the predicted field dependence (Fig. 8). Surprisingly it fades by approaching the field of ~5 T, and no resonance signals could be found at smaller fields. Such peculiar absence of resonance modes in the low field regime is in a remarkable correspondence with the vanishing of the specific heat anomaly below ~ 5 T, which again points at the pronounced spin fluctuations in the magnetically ordered state which can be suppressed by magnetic field.

D. Nuclear magnetic resonance (NMR)

NMR on ^{75}As nuclei was measured with a Tecmag pulse solid-state NMR spectrometer with a 9.2 T superconducting magnet from Magnex Scientific. The NMR spectra were obtained by measuring the intensity of the Hahn echo versus magnetic field. The T_1 relaxation time was measured with the method of stimulated echo.

Representative ^{75}As NMR spectra for the *easy* axis *b* direction of the magnetic field are shown in Fig. 9. The temperature dependence of the ^{75}As spin lattice relaxation rate T_1^{-1} divided over T is shown in Fig. 10. In this figure, it is compared with the T dependence of the static susceptibility $\chi(T)$. The fact that both $(T_1 T)^{-1}$ and $\chi(T)$ follow closely the same temperature behavior suggests an appreciable coupling of the ^{75}As nuclei to the Cu spin system. In this case, the nuclear spin lattice relaxation is usually governed by magnetic fluctuations in the electronic spin system, and $(T_1 T)^{-1}$ is
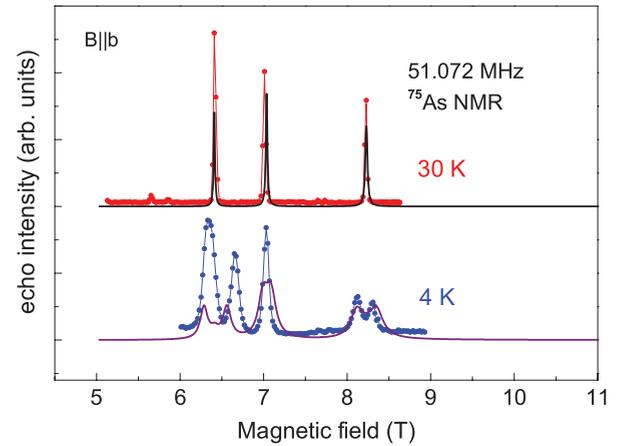
FIG. 9. (Color online) ^{75}As NMR spectra (dots) measured at 30 K and 4 K for the magnetic field direction parallel to the *b*-axis. Solid lines represent simulated spectra (see the text).

proportional to the imaginary part of the dynamic susceptibility χ'':

$$(T_1 T)^{-1} \propto \sum_{\vec{q}} A_\perp^2(\vec{q},\omega) \cdot \frac{\chi''(\vec{q},\omega)}{\omega}. \quad (1)$$

Here A is the hyperfine constant, q is the wave vector, and ω is the NMR frequency. Note a sharp peak of $(T_1 T)^{-1}$ at the ordering temperature T_N manifesting a critical behavior of Cu spin fluctuations (Fig. 10). At $T > T_N$, the ^{75}As NMR spectrum consists of three quadrupole-split lines as expected for nuclei with the spin $I = 3/2$ (Fig. 9). The spectrum has been modeled on the basis of the following Hamiltonian:[17]

$$\mathcal{H} = \frac{1}{6} h\nu_Q^z [3I_z^2 - I(I+1) + \frac{1}{2}\eta(I_+^2 + I_-^2)] + \gamma\hbar\mathbf{I} \cdot \mathbf{B}. \quad (2)$$

The first term here describes the quadrupole interaction and the second term the Zeeman interaction. A good agreement with the experiment has been achieved with the value of the quadrupole frequency $\nu_Q = 23$ MHz and the asymmetry
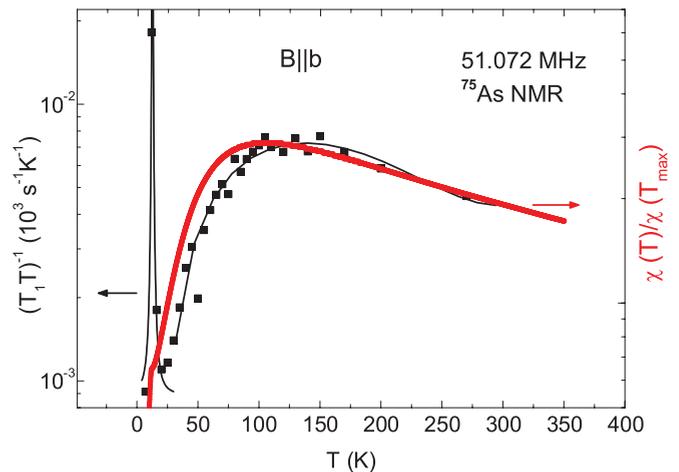
FIG. 10. (Color online) Temperature dependence of the ^{75}As spin lattice relaxation rate $(T_1^{-1} T)^{-1}$ in comparison with the static susceptibility. Thin solid line is the guide for the eye.

parameter $\eta = 0.1$. In the magnetically ordered state ($T < T_N$), the spectral lines experience a splitting into two components suggesting the occurrence of two nonequivalent magnetic environments of the ^{75}As nuclei. This can be related to the occurrence of two spin sublattices in the ordered Cu chains which exert alternating in sign internal field at the As sites. The low temperature NMR spectra can be successfully modeled on the basis of Hamiltonian (2) with the same values of ν_Q and η assuming two magnetically nonequivalent As sites (Fig. 9). The modeling yields the magnitude of the internal field at the ^{75}As amounting to $B_{int} = 0.3$ T, which is directed approximately perpendicular to the b axis. The substantially large value of B_{int} suggests a transferred nature of the internal field due to the overlap of electronic orbitals.

The finding that $B_{int} \perp b$ enables a conclusion that though the NMR has been measured at fields ~7 T substantially stronger that the spin-flop field $B_{SF} \simeq 1.7$ T, the Cu spins in the chains are still oriented predominantly perpendicular to the *easy* axis. This suggests the AFM exchange interaction between the Cu spins to be much stronger compared to the Zeeman energy, which renders the spin canting in a field of ~7 T very small. This complies with the small magnetization values shown in Fig. 4.

E. Density functional band structure calculations

DFT calculations have been performed using the full-potential code FPLO-8.50-32.[18] For the exchange and correlation potential, the scalar-relativistic parametrization of Perdew and Wang has been used.[19] The k mesh of 1152 points (320 in the irreducible wedge) has been adopted for the nonmagnetic calculations. The transfer integrals t_i have been evaluated based on a one-orbital tight-binding model, parameterized using Wannier functions. Strong electronic correlations are accounted for on a model level by resorting to a Hubbard model. At half-filling, the low-energy (magnetic) sector of this model is effectively described by a Heisenberg model.[20] Antiferromagnetic exchange integrals J_i^{AFM} have been determined based on transfer integrals t_i, adopting the second-order perturbation theory expression $J_i^{AFM} = 4t_i^2/U_{eff}$. Alternatively, the local (spin) density approximation has been used to evaluate the values of total exchange, comprising AFM as well as ferromagnetic (FM) contributions: $J_i = J_i^{AFM} + J_i^{FM}$. The k meshes used for LSDA + U supercell calculations number 12, 18, or 32 points, depending on the supercell size. The results were accurately checked for convergence.

Typical for cuprates, the valence band of α-Cu$_2$As$_2$O$_7$ is dominated by Cu and O states (Fig. 11). The nonzero density at the Fermi level evidences a metallic ground state, in contrast to the olive color of α-Cu$_2$As$_2$O$_7$ crystals. This discrepancy, typical for the LDA, originates from insufficient treatment of strong electronic correlations, intrinsic for the $3d^9$ electronic configuration of Cu^{2+}. Despite the inappropriate treatment of electron interaction terms, LDA correctly accounts for kinetic (exchange) processes, and thus can be used to derive the relevant orbitals and couplings. This way, we find that the magnetic properties of α-Cu$_2$As$_2$O$_7$ are governed by a Cu $3d$ orbital of the x^2-y^2 symmetry.[39] For these states, the Wannier functions are constructed.[22]
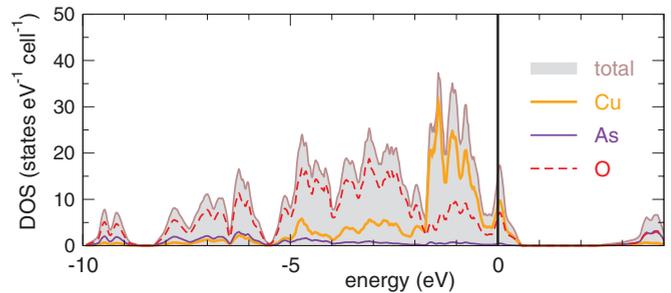
FIG. 11. (Color online) LDA total and atomic-resolved density of states of α-Cu$_2$As$_2$O$_7$. The main contribution to the valence band is due to Cu and O states (full orange and dashed red line, respectively). The Fermi level is at zero energy.

The analysis based on Wannier functions yields four relevant (>30 meV) transfer integrals. The leading terms are intra- and interdimer couplings t_1 and t_1', forming alternating chains running along b. In addition, the chains are coupled together by two inequivalent transfer integrals t_{ic1} and t_{ic3} shaping a 2D spin lattice (Fig. 12). Numerical values of the relevant t_i terms are given in Table I (third column).

Mapping onto a Hubbard model and subsequently onto a Heisenberg model yields the values of J_i^{AFM} (Table I). Considering $T_{max} = 105$ K from our $\chi(T)$ measurements, the large $J_1^{AFM} = 298$ K resulting from a typical value $U_{eff} = 4.5$ eV hints at a substantial FM contribution to this exchange. To evaluate the values of the total exchange J_i, we perform LSDA + U calculations. This calculational scheme adds correlations on top of the L(S)DA in a mean-field way. The implementation of the method relies on several parameters, namely, the on-site intraorbital term U_d, the on-site interorbital term J_d, and the particular way of accounting for the part of correlation energy already present in LDA. The latter term is typically referred as the double-counting correction (DCC), and two most widely used schemes are the around-mean-field (AMF), which uses a uniform orbital occupation as a reference, and the fully localized limit (FLL), referring to integer (0 or 1) occupation numbers.[23] For U_d, we
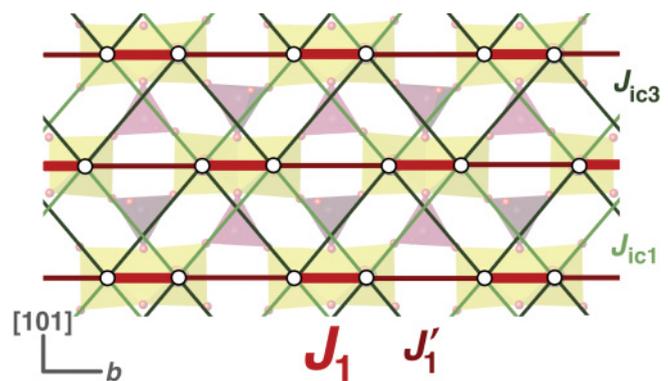
FIG. 12. (Color online) Microscopic spin model for α-Cu$_2$As$_2$O$_7$. Magnetic layers are formed by alternating $J_1 - J_1'$ chains running along b that are coupled by two inequivalent couplings J_{ic1} and J_{ic3}. The leading coupling J_1 corresponds to the magnetic exchange within the structural Cu$_2$O$_6$ dimers.

TABLE I. Leading couplings in α-Cu$_2$As$_2$O$_7$: Cu-Cu distance d (in Å), transfer integrals t_i (in meV), and AFM exchange integrals J_i^{AFM} (in K), calculated adopting $U_{\mathrm{eff}} = 4.5$ eV. Total exchange integrals J_i (in K) are evaluated from LSDA + U calculations adopting AMF ($U_d = 6.5$ eV) and FLL ($U_d = 9.0$ eV) DCC. The paths are depicted in Fig. 12.

Path	d	t_i	J_i^{AFM}	J_i, AMF	J_i, FLL
J_1	3.086	170	298	167	188
J_1'	5.239	104	112	125	102
J_{ic1}	6.437	76	60	44	42
J_{ic3}	6.465	77	61	46	42

used the range 6.5 ± 1 eV within AMF and 8.5 ± 1 eV within FLL, keeping $J_d = 1$ eV constant.

Representative values of the resulting J_i are given in Table I.[40] In agreement with the Goodenough-Kanamori rules,[25,26] the Cu-O-Cu angle of $101.7°$ leads to sizable FM contribution, and consequently, to a substantial reduction of J_1. However, in contrast to the isostructural compounds α-Cu$_2$P$_2$O$_7$ (Ref. 5) and β-Cu$_2$V$_2$O$_7$ (Ref. 4), this FM contribution does not suffice to reduce J_1 strongly, thus it remains the leading coupling in α-Cu$_2$As$_2$O$_7$. FM contributions to other relevant couplings are substantially smaller due to their long-range nature.

The interchain coupling topology in α-Cu$_2$As$_2$O$_7$ is similar to α-Cu$_2$P$_2$O$_7$, but contrasts to β-Cu$_2$V$_2$O$_7$. As discussed in Ref. 5, this essential difference originates from the nature of the atom residing in the center of anionic tetrahedra, in particular, whether it is a p element (P, As) or a d element (V). The former case favors the Cu-O-O-Cu connections via single tetrahedra, i.e., J_{ic1} and J_{ic3}.

To summarize the results of the band structure calculations, the microscopic magnetic model of α-Cu$_2$As$_2$O$_7$ features alternating spin chains, with both nearest-neighbor couplings AFM, and the dominant coupling J_1 within the structural Cu$_2$O$_6$ dimers. The chains are coupled by two inequivalent interchain couplings, forming a 2D nonfrustrated model.

F. QMC model studies

DFT calculations typically provide numerically accurate spin models, with surprisingly small errors for the individual exchange integrals J_i. Aiming to evaluate a quantitative microscopic magnetic model with even higher precision, we perform QMC simulations of the observed quantities and subsequently compare them to the experiments (Fig. 13).[27] We first attempt to describe the magnetic susceptibility of α-Cu$_2$As$_2$O$_7$ for $B \| b$ using the parameterized solution[28] for the alternating Heisenberg chain, valid in the temperature range $0.1 J_1 k_{\mathrm{B}}^{-1} \leqslant T \leqslant 4 J_1 k_{\mathrm{B}}^{-1}$. The fit exhibits good agreement with the experimental curve down to ~ 40 K, yielding $J_1 = 174$ K and $J_1' = 112$ K that conform to our LSDA + U results. However, the fitted value of g-factor amounts to only 1.94, strongly underestimating the intrinsic value of 2.07 derived from ESR.

Next, we take the interchain couplings into account. This way, we calculated the reduced magnetic susceptibility χ^* using QMC simulations of the spin Hamiltonian by consid-
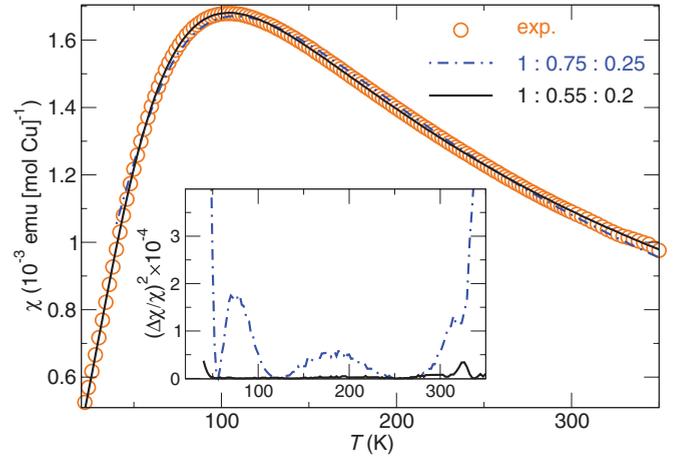
FIG. 13. (Color online) QMC fits to the experimental (exp.) magnetic susceptibility. The $J_1 : J_1' : J_{\mathrm{ic1}}$ ratios are given in the legend. The difference plots (inset) indicate the relative goodness of fit $(\Delta\chi/\chi)^2$ for the two parameter sets of $J_1 : J_1' : J_{\mathrm{ic1}}$.

ering finite lattices of $N = 2048$ sites (32 coupled chains of 64 spins each) with periodic boundary conditions. We used the stochastic series expansion algorithm implemented in the code LOOP[29] from the software package ALPS.[30] Low statistical errors (below 0.1%) are ensured by using 50 000 sweeps for thermalization and 500 000 steps after thermalization. The resulting simulated $\chi^*(T^*)$ dependencies were fitted to the experimental $\chi(T)$ curve using the expression:

$$\chi(T) = \frac{N_{\mathrm{A}} g^2 \mu_{\mathrm{B}}^2}{k_{\mathrm{B}} J_1} \cdot \chi^* \left(\frac{T}{k_{\mathrm{B}} J_1} \right) + \chi_0, \qquad (3)$$

where χ_0 is the temperature-independent contribution, and N_{A} and μ_{B} are the Avogadro constant and the Bohr magneton, respectively.

As a starting point, we adopt the ratios $J_1 : J_1' : J_{\mathrm{ic1}} = 1 : 0.75 : 0.25$ from the LSDA + U AMF calculations (Table I, last-but-one column). Although the resulting fit reasonably agrees with the experimental curve, small deviations evidence notable differences between our microscopic model and the experimental data. To adjust the model parameters, we varied J_1'/J_1 and J_{ic1}/J_1 ratios in a broad range, while the two relevant interchain couplings J_{ic1} and J_{ic3} were kept equal. This way, the best fit is attained for $J_1 : J_1' : J_{\mathrm{ic1}} = 1 : 0.55 : 0.20$, in almost perfect agreement with the ratios $1 : 0.54 : 0.22$ from the FLL DCC of LSDA + U (Table I, last column), with the absolute value of $J_1 = 164$ K only 13% smaller than its LSDA + U FLL estimate. Even more remarkable, the QMC fit yields $g = 2.06$, in excellent agreement with the experimental ESR estimate of 2.07 for $B \| b$. Therefore, the QMC simulations reveal crucial importance of interchain couplings for a proper description of the thermodynamic properties of α-Cu$_2$As$_2$O$_7$.

To investigate the role of interchain couplings for the magnetically ordered ground state, we calculate diagonal spin correlations $\langle S_0^z S_R^z \rangle$ for $0 \leqslant R \leqslant 6$ along different paths on the spin lattice (Fig. 14, right panel). First, we address the correlations between the alternating J_1-J_1' chains (Fig. 14, dashed and thin solid lines). As expected, J_{ic1} and J_{ic3} give rise to substantial interchain correlations, and thus favor a quasi-2D magnetic model. However, the correlations along the J_1-J_1'
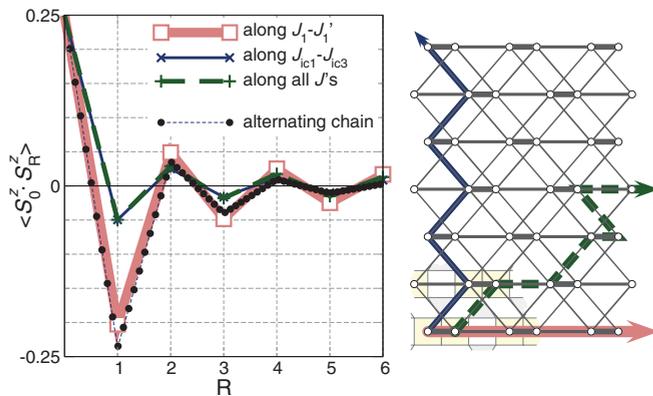
FIG. 14. (Color online) Left panel: diagonal spin correlations $\langle S_0^z S_R^z \rangle (R)$ in the magnetic ground state of $Cu_2As_2O_7$. The correlations along J_1-J_1' bonds (thick solid line, empty squares) closely resemble those of an alternating Heisenberg chain with $J_1':J_1 = 0.55$ (dotted line). In contrast, the correlations between the J_1-J_1' chains are substantially smaller (dashed and thin solid lines). Right panel: 0-R pathes in the spin lattice of $Cu_2As_2O_7$ used for the $\langle S_0^z S_R^z \rangle (R)$ plot in the left panel.

alternating chains (Fig. 14, thick line) nearly coincide with the spin correlations of an alternating Heisenberg chain featuring the same ratio (0.55) of the nearest-neighbor couplings (Fig. 14, dotted line). Therefore, the interchain couplings, despite their crucial role for long-range magnetic ordering, have only a minor impact on the key element of the magnetic model—J_1-J_1' alternating spin chains. As a result, even the purely 1D J_1-J_1' model reasonably fits the experimental magnetic susceptibility, although the underestimated g value and the magnetic transition at T_N evidence notable deviations from such a simplified model.

G. Structure-property relationships

Since continuous symmetries can not be spontaneously broken at finite temperature neither in one nor in two dimensions,[31] the observed long-range AFM order below $T_N = 10$ K can be accounted for only by extending the model with an effective coupling between the magnetic layers. Considering the small size of this coupling, its accurate estimate based on DFT results is at best challenging. In addition, the propagation vector of the magnetically-ordered structure is not known, impeding a conclusive analysis of the interchain coupling regime on a microscopic level. Therefore, the magnetic ordering temperature as well as the propagation vector are beyond the scope of the present study.

Magnetic layers formed by coupled structural dimers are a common element in spin-$\frac{1}{2}$ systems based on Cu^{2+} [α-$Cu_2P_2O_7$ (Ref. 5) and β-$Cu_2V_2O_7$ (Ref. 4)] as well as V^{4+} [$(VO)_2P_2O_7$ (Ref. 34), CsV_2O_5 (Ref. 33), and $VOSeO_3$ (Ref. 34)]. A key feature of their microscopic magnetic models is the minor role of the coupling J_1 within structural dimers, compared to the stronger coupling running via the double bridge of nonmagnetic anions between the structural dimers (J_1' in our present notation).[35] The reduction in J_1 is generally understood as the suppression of Cu-O-Cu or

V-O-V superexchange due to a bond angle slightly exceeding $90°$. In contrast, α-$Cu_2As_2O_7$ stands out against this trend, since the dominating coupling J_1 is restored unexpectedly. The enhanced value of $J_1 \simeq 164$ K is only partially related to the change in the Cu-O-Cu bond angle that amounts to $101.7°$, compared to $100.4°$ in α-$Cu_2P_2O_7$ ($J_1 \simeq 30$ K)[5] and $98.7°$ in β-$Cu_2V_2O_7$ ($J_1 \leqslant 12$ K).[4] An efficient mechanism affecting the coupling could be the polarization of particular oxygen $2p$ orbitals by As states, as proposed for Ge^{4+} in $CuGeO_3$.[36] A microscopic investigation of other Cu^{2+} arsenates will help to clarify this issue.

The coupling regime of α-$Cu_2As_2O_7$ underscores the wide diversity of spin lattices arising from the quasi-1D arrangement of structural dimers. Apart from the aforementioned Cu^{2+} and V^{4+} compounds, a similar structural feature is found in $Cu_2(PO_3)_2CH_2$ (Ref. 37) and $VOHPO_4 \cdot 0.5H_2O$ (Ref. 38). Altogether, these compounds exhibit remarkably different ground states, dimensionality, and even frustration regimes: Compare, for example, the spin gap in the quasi-1D $(VO)_2P_2O_7$ to the long-range magnetic order in the quasi-2D β-$Cu_2V_2O_7$, and further to the quasi-2D frustrated $Cu_2(PO_3)_2CH_2$ that again features a singlet ground state. α-$Cu_2As_2O_7$ takes its own distinct position in this series as a quasi-1D nonfrustrated system exhibiting a magnetic ordering transition at the notably low $T_N/J_1 \simeq 0.06$.

IV. CONCLUSIONS

The magnetic properties of α-$Cu_2As_2O_7$ single crystals have been investigated using several experimental methods (static susceptibility, magnetization, heat capacity, ESR, and NMR measurements), as well as density-functional band-structure calculations and QMC simulations. The results show that α-$Cu_2As_2O_7$ is a spin-$1/2$ low-dimensional system with the crystallographic b axis as the magnetically *easy* axis. The intrachain interactions are reflected in 1D short range AFM correlations below $\sim$100 K and short range magnetic ordering below $\sim$60 K. A significant interchain coupling contribution drives the system into an AFM long range order at $T_N \simeq 10$ K. We find that a second phase transition of spin-flop type takes place at $T < T_N$ for $B_{SF} \simeq 1.7$ T (2 K), most likely related to the gain in magnetic anisotropy energy. The collinear AF magnetic ordering below B_{SF} is confirmed by a well defined λ-like anomaly in the magnetic specific heat quantity. On the contrary, neither specific heat shows the expected λ-like specific heat anomaly below $\sim$5 T, nor are ESR signals detectable in this low field range suggesting the occurrence of strong spin fluctuations at small fields. The occurrence of the AFM resonance mode and the splitting of the ^{75}As NMR signals observed in the high field regime suggests the robust AFM spin order in the spin flop phase above $\sim$5 T. The DFT calculations yield a reliable determination of all relevant magnetic couplings. A combined analysis of experimental and theoretical data enables a conclusion that, in contrast to other isostructural compounds, the pyroarsenate α-$Cu_2As_2O_7$ can be effectively described by a *coupled* alternating Heisenberg chain model with the leading intrachain coupling placed within the structural dimers Cu_2O_6. The topology and the strength of exchange couplings determined from DFT calculations render

a spin frustration scenario unlikely and rather put forward low-dimensional nature of the spin system. We conclude that indeed the electronic state of the central ion in the nonmagnetic AsO_4 side groups plays a crucial role for determining the relevant interchain pathways which makes α-$Cu_2As_2O_7$ distinct in its magnetic properties from other representatives of this class of compounds.

[1] R. Wyckoff, *Crystal Structures*, Vol. 3 (Wiley Interscience, New York, 1960).

[2] J. S. Gardner, M. J. P. Gingras, and J. E. Greedan, Rev. Mod. Phys. **82**, 53 (2010).

[3] J. Pommer, V. Kataev, K.-Y. Choi, P. Lemmens, A. Ionescu, Y. Pashkevich, A. Freimuth, and G. Güntherodt, Phys. Rev. B **67**, 214410 (2003).

[4] A. A. Tsirlin, O. Janson, and H. Rosner, Phys. Rev. B **82**, 144416 (2010).

[5] O. Janson, A. A. Tsirlin, J. Sichelschmidt, Y. Skourski, and H. Rosner, e-print arXiv:1011.5393v2.

[6] *Quantum Magnetism*, Lecture Notes in Physics, edited by U. Schollwöck, J. Richter, D. Farnell, and R. Bishop, Vol. 645 (Springer, New York, 2004).

[7] A. M. Buckley, S. T. Bramwell, P. Day, and D. Visser, J. Solid State Chem. **115**, 229 (1995).

[8] M. Weil, C. Lengauer, E. Füglein, and E. J. Baran, Cryst. Growth and Design **4**, 1229 (2004).

[9] M. E. Fisher, Proc. R. Soc. London A **254**, 66 (1960).

[10] M. E. Fisher, Phil. Mag. **7**, 1731 (1962).

[11] R. Klingeler, J. Geck, R. Gross, L. Pinsard-Gaudart, A. Revcolevschi, S. Uhlenbruck, and B. Büchner, Phys. Rev. B **65**, 174404 (2002).

[12] A. Tari, *The Specific Heat of Matter at Low Temperatures* (Imperial College Press, London, 2003).

[13] C. Golze *et al*., Phys. Rev. B **73**, 224403 (2006).

[14] A. Abragam and B. Bleaney, New. J. Chem. **11**, 321 (1987).

[15] R. Klingeler, B. Büchner, K.-Y. Choi, V. Kataev, U. Ammerahl, A. Revcolevschi, and J. Schnack, Phys. Rev. B **73**, 14426 (2006).

[16] E. A. Turov, *Physical Properties of Magnetically Ordered Crystals*, edited by A. Tybulewicz and S. Chomet (Academic Press, New York and London, 1965).

[17] A. Abragam, *Principles of Nuclear Magnetism* (Oxford University Press, Oxford, 1961).

[18] K. Koepernik and H. Eschrig, Phys. Rev. B **59**, 1743 (1999).

[19] J. P. Perdew and Y. Wang, Phys. Rev. B **45**, 13244 (1992).

[20] P. W. Anderson, Phys. Rev. **115**, 2 (1959).

[21] The x axis of this local coordinate system runs along one of the Cu-O bonds, the z axis is perpendicular to the plaquette plane.

[22] H. Eschrig and K. Koepernik, Phys. Rev. B **80**, 104503 (2009).

[23] E. R. Ylvisaker, W. E. Pickett, and K. Koepernik, Phys. Rev. B **79**, 035103 (2009).

[24] The ratios of the leading couplings in the final model are mostly independent of the particular choice of U_d and DCC, although differences in the values of individual exchange couplings are of the order of 30%.

[25] J. B. Goodenough, Phys. Rev. **100**, 564 (1955).

[26] J. Kanamori, J. Phys. Chem. Solids **10**, 87 (1959).

[27] A. A. Tsirlin and H. Rosner, Phys. Rev. B **82**, 060409 (2010); O. Janson, A. A. Tsirlin, and H. Rosner, *ibid*. **82**, 184410 (2010).

[28] D. C. Johnston, R. K. Kremer, M. Troyer, X. Wang, A. Klümper, S. L. Bud'ko, A. F. Panchula, and P. C. Canfield, Phys. Rev. B **61**, 9558 (2000).

[29] S. Todo and K. Kato, Phys. Rev. Lett. **87**, 047203 (2001).

[30] A. Albuquerque, F. Alet, P. Corboz, P. Dayal, A. Feiguin, S. Fuchs, L. Gamper, E. Gull, S. Gürtler, A. Honecker, R. Igarashi, M. Körner, A. Kozhevnikov, A. Läuchli, S. R. Manmana, M. Matsumoto, I. P. McCulloch, F. Michel, R. M. Noack, G. Pawlowski, L. Pollet, T. Pruschke, U. Schollwöck, S. Todo, S. Trebst, M. Troyer, P. Werner, and S. Wessel, J. Magn. Magn. Mater. **310**, 1187 (2007).

[31] N. D. Mermin and H. Wagner, Phys. Rev. Lett. **17**, 1133 (1966).

[32] D. C. Johnston, J. W. Johnson, D. P. Goshorn, and A. J. Jacobson, Phys. Rev. B **35**, 219 (1987); M.-J. Cheng, R. J. Nielsen, J. Tahir-Kheli, and W. A. G. III, PhysChemChemPhys **13**, 9831 (2011).

[33] R. Valentí and T. Saha-Dasgupta, Phys. Rev. B **65**, 144445 (2002). A. Saúl and G. Radtke, Phys. Rev. Lett. **106**, 177203 (2011). Y. Ueda, Chem. Mater. **10**, 2653 (1998).

[34] J.-C. Trombe, A. Gleizes, J. Galy, J.-P. Renard, Y. Journaux, and M. Verdaguer, New J. Chem. **11**, 321 (1986); R. Valentí, T. Saha-Dasgupta, and F. Mila, Phys. Rev. B **68**, 024411 (2003).

[35] A. W. Garrett, S. E. Nagler, D. A. Tennant, B. C. Sales, and T. Barnes, Phys. Rev. Lett. **79**, 745 (1997).

[36] W. Geertsma and D. Khomskii, Phys. Rev. B **54**, 3011 (1996).

[37] M. Schmitt, A. A. Gippius, K. S. Okhotnikov, W. Schnelle, K. Koch, O. Janson, W. Liu, Y.-H. Huang, Y. Skourski, F. Weickert, M. Baenitz, and H. Rosner, Phys. Rev. B **81**, 104416 (2010).

[38] D. A. Tennant, S. E. Nagler, A. W. Garrett, T. Barnes, and C. C. Torardi, Phys. Rev. Lett. **78**, 4998 (1997); S. Petit, S. Borshch, and V. Robert, Inorg. Chem. **43**, 4210 (2004); J. Cao, J. T. Haraldsen, S. Brown, J. L. Musfeldt, J. R. Thompson, S. Zvyagin, J. Krzystek, M.-H. Whangbo, S. E. Nagler, and C. C. Torardi, Phys. Rev. B **72**, 214421 (2005).

[39] The x-axis of this local coordinate system runs along one of the Cu–O bonds, the z axis is perpendicular to the plaquette plane.

[40] The ratios of the leading couplings in the final model are mostly independent of the particular choice of U_d and DCC, although differences in the values of individual exchange couplings are of the order of 30%.